JOURNAL OF GEOPHYSICAL RESEARCH, VOL. 100, NO. D4, PAGES 7121–7133, APRIL 20, 1995

Numerical modeling of ship tracks produced by injections of cloud condensation nuclei into marine stratiform clouds

Andrew S. Ackerman,[1] Owen B. Toon,[2] and Peter V. Hobbs[1]

Abstract. Ship tracks are long-lived, linear regions of enhanced reflectivity in low-lying marine clouds that appear in satellite imagery downwind of ships. Ship tracks were first observed as cloud lines in visible satellite imagery (type 1). A second (and more common) type of ship track (type 2), which is masked at visible wavelengths by natural variability in cloud reflectivity, is seen at near-infrared wavelengths in satellite imagery. A one-dimensional numerical model is used to simulate measurements of both types of ship tracks and to investigate interactions between aerosol and cloud microphysics, radiative transfer, and turbulent mixing in the cloud-topped marine boundary layer that lead to the formation and provide for the persistence of ship tracks. We find that cloud condensation nuclei (CCN) injections can account for many of the observed properties of ship tracks. Higher CCN concentrations produce increased droplet concentrations, which enhance cloud reflectivity by reducing droplet radius and increasing droplet cross-sectional area. The smaller droplets also reduce the drizzle rate, which can allow cloud water to increase under some conditions, thereby leading to higher cloud reflectivity. However, smaller droplets also evaporate more readily below cloud base. Increased evaporation reduces mixing between the cloud and the subcloud layers during daytime, which causes a decrease in cloud water. The distinction between the two types of ship tracks is suggested to be due to differences in ambient concentrations of CCN that cause variations in turbulent mixing in the boundary layer, through the effect of cloud droplet concentrations on cloud-top longwave radiative cooling. The model predicts lifetimes of > 1 day and > 2 days for the simulated type 1 and type 2 ship tracks, respectively. In the atmosphere, processes not treated in the model, such as horizontal dispersion and changes in large-scale atmospheric conditions, may limit ship track lifetimes.

1. Introduction

Ship tracks are long-lived, linear regions of enhanced solar reflectivity in marine stratiform clouds that appear in satellite imagery downwind of ships. They were first reported as "anomalous cloud lines" in visible satellite imagery [*Conover*, 1966]. The cloud cover in the regions in which the features were observed ranged from apparently cloud-free to overcast, where the lines became indiscernible. Conover concluded that the cloud lines were low-lying water clouds, resulting from the addition of CCN present in ship exhausts under special meteorological conditions; *Bowley* [1967] observed that these cloud lines were typically associated with fog in a shallow boundary layer. Conover suggested that the ambient air in which ship tracks form must have very low concentrations of CCN; *Twomey et al.* [1968] reported that very low CCN concentrations (< 5 cm^{-3}) are sometimes measured in areas where ship tracks occur. Using multiple wavelength detectors on modern satellites, *Coakley et al.* [1987] expanded the definition of ship tracks to include radiative perturbations within optically thick cloud layers. They reported that ship tracks are detected more readily in satellite imagery of marine stratocumulus clouds at near-infrared wavelengths (3.7 μm) than at visible wavelengths, because at visible wavelengths, ship tracks are often masked by large variabilities in the reflectivity of the surrounding cloud. In this study we will refer to ship tracks detectable in visible satellite imagery as type 1. Ship tracks that are embedded in optically thick cloud layers and are detectable most easily in near-infrared satellite imagery will be referred to as type 2.

Ship tracks have been called the Rosetta Stone of aerosol-cloud-climate interactions because they serve as a striking example of the effects of increased CCN concentrations on the albedo of marine stratiform clouds [*Porch et al.*, 1990]. Because marine stratiform clouds overlie about a third of the oceans and reflect much more solar energy than the ocean surface, they play an important role in the global radiative heat balance [*Warren et al.*, 1988]. *Randall et al.* [1984] estimated that a 4% increase in the global coverage of marine stratiform clouds (corresponding to an increase in marine stratiform cloudiness of ~15%) could offset the radiative forcing expected from a doubling of atmospheric carbon dioxide. Improved understanding of the mechanisms for the formation and persistence of ship tracks should provide insights into the potential effects on global climate of large-

[1] Department of Atmospheric Sciences, University of Washington, Seattle.

[2] Space Science Division, NASA Ames Research Center, Moffett Field, California.

Paper number 95JD00026.
0148-0227/95/95JD-00026$05.00

scale increases in aerosol concentrations through their effects on clouds.

It has been suggested that perturbations other than increased CCN concentrations might be involved in the formation and maintenance of ship tracks. Other possible perturbations include heat from ships [*Porch et al.*, 1990] and air wake vortices behind ships [*Hindman*, 1990]. However, we will confine our attention to the effects of CCN injections on warm, stratiform clouds in the marine boundary layer.

In this paper we use a numerical model to see if reasonable injections of particles into the marine boundary layer can account for ship tracks, to investigate some of the processes responsible for the formation and persistence of ship tracks, and to investigate mechanisms that might be responsible for the differences between type 1 and type 2 ship tracks. However, we will start by discussing some theories for interactions between aerosols and marine stratiform clouds. Then we summarize two sets of measurements on ship tracks. This is followed by a description of the numerical model that we have used in this study and the results of applying the model to simulate the two sets of ship track measurements.

2. Interactions Between Cloud Condensation Nuclei (CCN) and Clouds

2.1. Enhancement of Cloud Albedo Due to Increase in Droplet Cross-Sectional Area

In the first report of ship tracks, *Conover* [1966] concluded that the observed increase in visible cloud albedo (which he estimated to be an increase from 13 to 38%) could be explained if the total droplet concentration of a cloud increased from 30 to ~200 cm^{-3} (with cloud thickness and liquid water content remaining unchanged). A similar argument was put forth by *Twomey* [1974] who suggested that aerosol pollution in general can enhance cloud albedo. This argument is based on the fact that liquid water does not absorb visible radiation significantly; therefore cloud optical depth is proportional to the total droplet cross-sectional area (which scatters solar radiation), which increases with increasing droplet concentrations. Cloud albedo is dependent on cloud optical depth (τ) which can be approximated at visible wavelengths by [*Hansen and Travis*, 1974]

$$\tau = \frac{3W}{2r_{eff}} \tag{1}$$

where W is the vertically integrated liquid water path (in units of grams per square meter) and r_{eff} is the area-weighted effective radius of the droplets (in units of micrometers).

Coakley et al. [1987] found that the natural variability in the albedo of stratocumulus cloud fields (due to variations in W and r_{eff}) generally masked any visible enhancement of cloud reflectivity due to ships. However, they detected ship tracks in stratocumulus cloud layers at the near-infrared wavelength of 3.7 μm. The scattering of near-infrared radiation is also proportional to the total droplet cross-sectional area, but because liquid water absorbs a fraction of incident radiation at near-infrared wavelengths (unlike visible radiation), absorption is proportional to the total droplet volume. Hence the ratio of scattering to absorption of near-infrared radiation increases as the average droplet size decreases. This dependence of the ratio of scattering to absorption at near-infrared wavelengths on r_{eff} results in the enhanced reflectivity of ship tracks at 3.7 μm.

2.2. Increases in Cloud Albedo and Lifetime Due to Decrease in Precipitation Efficiency

Albrecht [1989] suggested that by reducing the precipitation efficiency of marine stratiform clouds, increased CCN concentrations could increase cloud albedo and lifetime. In Albrecht's conceptual model, increased CCN concentrations lead to smaller droplets, which produce less drizzle because droplet collisions are reduced. Reduction in the removal rate of cloud water by drizzle should allow cloud water to rise, which will increase cloud albedo through its effect on the total droplet cross-sectional area. Albrecht reasoned that another effect of decreased drizzle is to increase mixing between the cloud and the subcloud layers. Increased mixing occurs because the evaporation of drizzle below cloud cools the air there, stabilizing it with respect to the cloud. With less drizzle, less stabilization occurs, thereby increasing the turbulent mixing between the cloud and the subcloud layers. Albrecht suggested that the increased mixing should increase cloud amount by increasing cloud lifetimes.

An increase in cloud water due to an increase in CCN concentration will enhance cloud albedo in ship tracks beyond that attributable to any increase in droplet concentration due to increased CCN concentration. An increase in cloud amount may further enhance the albedo of ship tracks, by filling in clear areas between clouds; this might explain *Scorer*'s [1987] observations of increased cloud amount in some ship tracks.

2.3. Increase in CCN Lifetime Due to Increase in CCN Concentrations

Ackerman et al. [1994] argued that CCN lifetime is proportional to CCN (and cloud droplet) concentration. This conclusion was based on results from numerical model simulations in which a source of CCN in the boundary layer was balanced by removal due to droplet collisions, thermal coagulation of haze particles, and deposition at the surface. They calculated an average CCN residence time for each simulation by dividing the equilibrium particle concentration (total of unactivated CCN and water droplets) by the CCN source strength. Because the equilibrium particle concentrations increased faster than the source strength in their calculations, the CCN lifetime increased with increasing CCN concentration. The increased lifetime occurs because the likelihood of a collision (per droplet) decreases as droplet size decreases. Therefore by decreasing their own removal rate, high CCN concentrations tend to be self-perpetuating. Persistence of high CCN concentrations may contribute to the long lifetimes of ship tracks.

2.4. Collapse of the Marine Boundary Layer Due to Depletion of CCN

Marine stratocumulus clouds are often optically thick enough to drive vertical mixing through cloud-top radiative cooling [*Lilly*, 1968]. This mixing provides moisture to the clouds and maintains the depth of the boundary layer against the subsidence of the overlying air. Droplet collisions can significantly reduce CCN concentrations in the marine boundary layer [*Hudson and Frisbie*, 1991; *Hudson*, 1993]. When droplet concentrations fall to very low values ($\lesssim 5$ cm^{-3}), a cloud layer can become optically thin enough for radiative cooling to spread over the depth of the cloud layer, and the location of the maximum cooling rate moves downward from cloud top. Thereafter the profile of radiative cooling

stabilizes the temperature profile of the upper region of the cloud layer, which can cause the boundary layer to collapse to a shallow, surface-driven, fog layer. In view of this possible chain of events, *Ackerman et al.* [1993] suggested that marine stratiform clouds can limit their own lifetimes by reducing CCN number concentrations. Conversely, an injection of CCN into such a collapsed boundary layer might initiate a chain of events that leads to a deepening of the boundary layer due to the creation of a long-lived, optically thick, stratiform cloud layer. Pronounced effects on boundary layer mixing due to changes in CCN concentrations are clearly relevant to ship tracks.

3. Field Measurements of Ship Tracks

We are aware of only two sets of field measurements on ship tracks. The first set resulted from an airborne penetration of a pair of ship tracks during the First ISCCP (International Satellite Cloud Climatology Project) Regional Experiment (FIRE) marine stratocumulus campaign off the coast of southern California around 0800 local standard time (LST) on July 13, 1987 [*Radke et al.*, 1989; *King et al.*, 1993]. Satellite observations of the area, made around the same time as the in situ measurements, revealed two linear cloud features ~200 km in length. At a wavelength of 0.63 μm the reflectivity of the ship tracks was 68% while that for the surrounding cloud was 61% [*Radke et al.*, 1989]. Because these ship tracks appeared in an area of optically thick clouds (with significant variations in reflectivity outside the ship tracks), we classify them as type 2. The in situ measurements were made while flying through the middle of a stratocumulus cloud layer about 400 m thick that topped a ~900-m-deep boundary layer. In the second ship track penetrated by the aircraft, the droplet concentration jumped from an average value of ~40 cm^{-3} in the surrounding clouds to ~120 cm^{-3} (averaged over the ~20-km width of the ship track); the effective radius of the droplet size distribution fell from ~12 to ~8 μm; and the liquid water content rose from 0.3 to 0.45 g kg^{-1}. The increase in droplet concentration and the corresponding decrease in droplet effective radius could have been direct consequences of the addition of CCN from a ship, and the increase in liquid water content could have been due to the suppression of drizzle.

The second set of ship track field measurements were taken from aboard a ship off the coast of Baja California, on July 13, 1991 [*Hindman et al.*, 1992]. A visible satellite image (wavelength = 0.63 μm) of this ship track is shown in Figure 1a. The research vessel passed under the visible ship track in the southern area of the image between 0900 and 1000 local standard time in the midst of a drizzling, broken stratus cloud layer that capped a shallow boundary layer (~500 m deep). We classify the ship track seen in the southern area of Figure 1a as type 1, because it stands out prominently in contrast to the optically thin, broken cloud field surrounding it. In the southern area of Figure 1a the ambient concentration of CCN active at 0.8% supersaturation was measured at the surface to be only 5 cm^{-3}. Beneath the ship track and ~40 km downwind of the ship that produced it, the CCN concentration at the surface jumped to 200 cm^{-3}; the corresponding CCN activation spectrum is shown in Figure 2. Analysis of 11-μm satellite data indicates that the top of the ship track protruded above the surrounding broken stratus layer [*Hindman et al.*, 1994]. Although not readily apparent

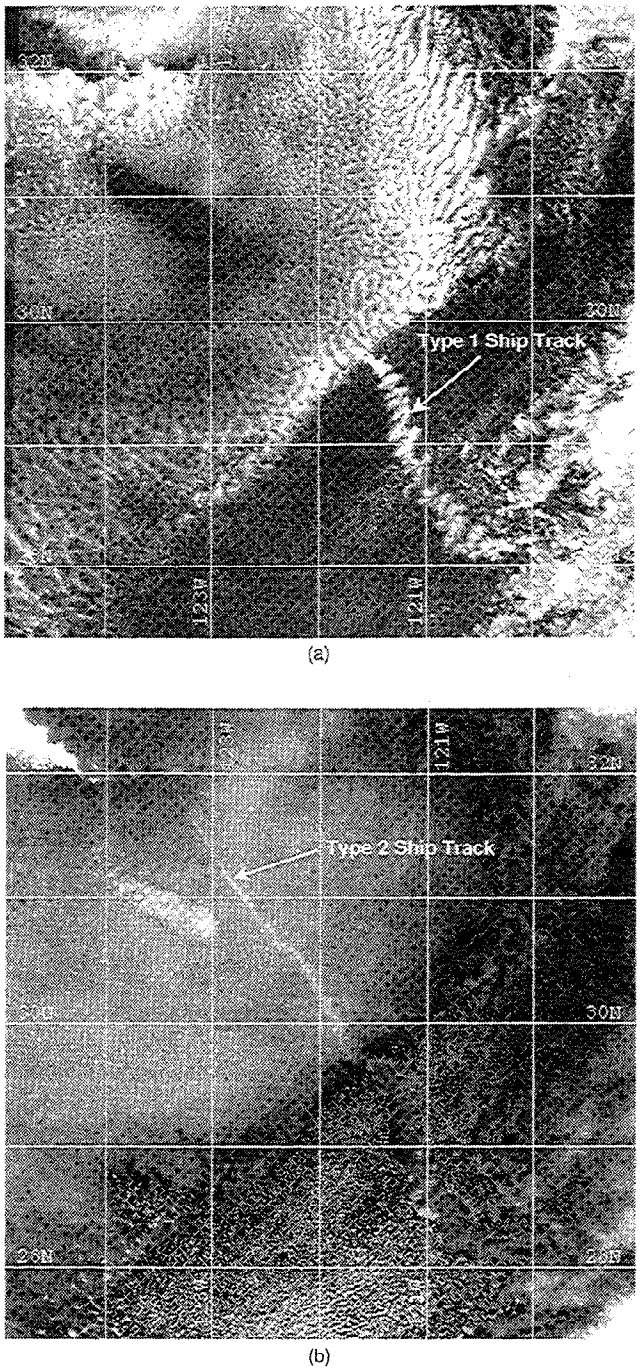

Figure 1. Imagery from the advanced very high resolution radiometer (AVHRR) on the polar orbiting NOAA 11 satellite taken at 1507 PDT on July 13, 1991, at wavelengths of (a) 0.63 and (b) 3.7 μm.

in the visible satellite image, the ship track observed by Hindman et al. extended into the optically thick stratus layer to the north, as revealed by near-infrared satellite imagery (wavelength = 3.7 μm) of the area, shown in Figure 1b. Because the ship track in the northern region seen in Figure 1b was embedded in an optically thick cloud layer and detectable only in near-infrared satellite imagery, we classify it as type 2. Underneath the stratus layer in this region, drizzle no longer reached the surface and ambient CCN concentrations were 60 cm^{-3}.

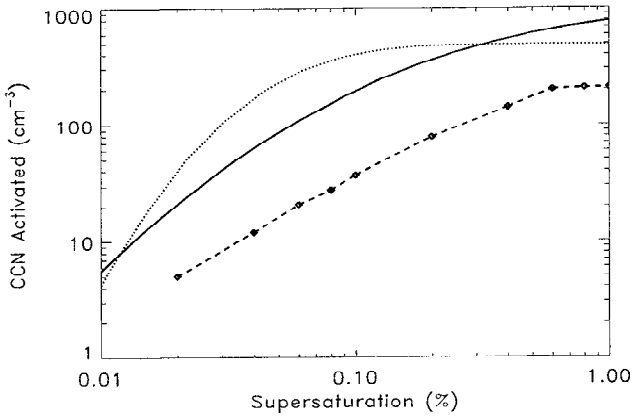

Figure 2. Comparisons of cumulative cloud condensation nuclei (CCN) activation spectra for the particle injections (solid line is for the type 1 ship track simulation and the dotted line is for the type 2 ship track simulation) with surface measurements taken under a type 1 ship track on July 13, 1991 (J. G. Hudson, unpublished data, 1993) (diamonds connected by dashed line). The values for the model simulations are averaged over the (modeled) boundary layer depths.

4. Numerical Model Simulations

4.1. Model Description

To investigate interactions between aerosols and cloud radiative properties, we have developed a numerical model of the stratocumulus-topped marine boundary layer [*Ackerman et al.*, 1995]. This one-dimensional model consists of three coupled components that treat aerosol and cloud microphysics, radiative transfer, and turbulent mixing. The aerosol and cloud physics component [*Toon et al.*, 1988] resolves the size distributions of both unactivated haze particles and activated cloud droplets and explicitly treats the warm cloud microphysical processes that affect them. Cloud optical properties and radiative heating rates are computed with the radiative transfer scheme of *Toon et al.* [1989]. Vertical transport is represented with a turbulent kinetic energy closure scheme [*Duynkerke and Driedonks*, 1987]. *Ackerman et al.* [1995] show that simulations from this model compare favorably with airborne measurements of marine stratiform clouds described by *Nicholls* [1984] and *Nicholls and Leighton* [1986].

For the model simulations the layer nearest the surface was 30 m thick, and layer thicknesses decreased upward to 10 m at the initial altitude of the inversion, above which the layer thickness was constant at 10 m. The size distributions of dry aerosol particles and droplets were each divided into fifty bins, with geometrically increasing size, resulting in a radius grid from 0.005 to 500 μm. Within each droplet size bin, the model solves continuity equations for the total volume of dissolved CCN and the second moment of the CCN volume distribution. The radiative transfer model treats multiple scattering over 26 wavelengths (0.26 to 4.3 μm) and absorption and scattering over 14 wavelengths (4.4 to 62 μm). For the radiative calculations the size distributions of aerosol particles are transformed from their dry to their equilibrium (wet) sizes at the ambient relative humidity. Aerosol particles that were below the smallest size activated as CCN in the model domain were ignored in the radiative calculations, in order to avoid the enhancement of cloud albedo due to artificially elevated concentrations of small particles in the simulated ship track plumes.

There are shortcomings inherent to the one-dimensional model because it averages over updrafts and downdrafts. For instance, peak supersaturations in the cloud layer are underpredicted by the model; consequently, the fraction of total aerosol particles activated as CCN is also underpredicted. To predict cloud droplet concentrations that are consistent with measurements, artificially high concentrations of aerosol particles are input to the model, as described below. Other aspects of the model simulations that may be artifacts of its one-dimensional formulation (e.g., supersaturation increases with height in the cloud layer, as does the total concentration of activated cloud droplets) are discussed in detail by *Ackerman et al.* [1995]. Although the model shortcomings result in some quantitative differences between measurements and model predictions, the qualitative responses of the model are probably realistic.

4.2. Design of Model Simulations

To simulate both sets of ship track observations, we initialized the model with a cloudless marine boundary layer at midnight, local time. By initializing the model domain as cloudless, the model was allowed to generate a cloud layer consistent with the model physics, thereby avoiding any initial assumptions about the simulated cloud layer. The initial and fixed conditions for the model simulations are summarized in Table 1. For all simulations the sea surface temperature was fixed at 17°C, and the air temperature at the midpoint of the lowest model layer (at 15 m altitude) was initially 1°C lower than the surface temperature. The initial temperature profile was adiabatic up to the initial altitude of the temperature inversion that caps the boundary layer (500 m for type 1, 900 m for type 2), and the initial relative humidity was 98.3% throughout the boundary layer. Above the inversion the temperature and the water vapor mixing ratio were initially independent of altitude (values are given in Table 1). The wind profiles were initialized at their geostrophic values, which are assumed to be independent of altitude. To limit upward entrainment of the boundary layer, a constant divergence rate of the horizontal winds was fixed at 3×10^{-6} s^{-1} for both simulations. The initial distributions of dry particles were independent of altitude and specified as lognormal distributions (with a geometric mean radius by number, r_n, of 0.05 μm, and a geometric standard deviation, σ, of 2.5) of ammonium bisulfate (the average composition of aerosol measured by *Covert* [1988] in the remote North Pacific boundary layer). The resulting slope of the CCN activation spectrum was chosen to generally match the measurements of *Hudson and Frisbie* [1991], which were obtained under marine stratiform clouds off the coast of southern California (for a comparison between measurements and the initial CCN spectrum, see *Ackerman et al.* [1995]). The initial number concentrations of particles and the (fixed) aerosol production rates are given in Table 1. Aerosol particles were created in the boundary layer (using the same distribution as in the initialization) throughout the simulations to offset the losses of particles due to aggregation and surface deposition; there was no source of particles from above the boundary layer due to subsidence. The initial concentrations and production rates

Table 1. Initial and Fixed Conditions for the Model Simulations

Parameter	Type 1	Type 2
Initial Conditions		
Inversion height, m	500	900
Vapor mixing ratio above inversion, g kg^{-1}	5	4.5
Temperature above inversion, °C	20.5	20
Downwelling longwave radiative flux above inversion, W m^{-2}	260	280
Dry particle size distribution		
total number concentration, cm^{-3}	20	500
geometric standard deviation	2.5	2.5
geometric mean radius, μm	0.05	0.05
Fixed Conditions		
Aerosol production rate, cm^{-3} s^{-1}	10^{-3}	8×10^{-3}
Sea surface temperature, °C	17	17
Geostrophic wind speed, m s^{-1}	10	5
Divergence rate of horizontal winds, s^{-1}	3×10^{-6}	3×10^{-6}
Latitude, deg	122°W	121°W
Longitude, deg	31°N	33°N
Date, for solar zenith angle	July 13	July 10

of particles were chosen to attain droplet or CCN concentrations (for the type 1 and type 2 simulations, respectively) approximately equal to the measured values in the uncontaminated boundary layers. No reliable data are available to constrain the downwelling longwave radiative fluxes at the inversion; the values used (Table 1) were chosen to maintain roughly constant boundary layer depths.

For each type of ship track, a model simulation was first run through a diurnal cycle with the fixed and initial conditions shown in Table 1. After this initialization period the model simulation for each type of ship track was split into a control run and a ship track run. In the control run, each model simulation was extended for a further 48 hours (beyond the initialization period) to represent the "natural" conditions. In the ship track run, a pulse of particles (representing pollution from a ship) was instantaneously injected into the model layer located 100 m above the surface. The ship track run was then extended for a further 48 hours to determine the effects of the pulse of particles.

For the particle injection in the type 1 ship track run we matched the CCN activation spectrum measured under the ship track using a lognormal distribution of ammonium bisulfate particles with r_n = 0.03 μm and σ = 2.5 (Figure 2). Matching the slope of an observed CCN activation spectra is equivalent to matching the shape of the observed aerosol size distribution (assuming the same solute composition). The particle injection in the type 1 ship track run (5×10^7 cm^{-2}) resulted in a larger total concentration of CCN (~700 cm^{-3} active at 0.8% supersaturation) averaged over the boundary layer than was measured at the surface (200 cm^{-3} at 0.8% supersaturation). No measurements of CCN in the ship track are available for the type 2 case. Therefore we again used a particle injection strength of 5×10^7 cm^{-2} but used a lognormal distribution of ammonium bisulfate particles with r_n = 0.1 μm and σ = 1.6, which produced an increase in the total aerosol concentration of 500 cm^{-3} (averaged over the depth of the boundary layer). We did not use the same particle size distribution that we used for the type 1 simulation because an insignificant fraction of the particles would have nucleated droplets in the type 2 simulation. This difference in nucleation is because the peak supersaturations reached in the type 2 simulation were lower than in the type 1 simulations, due to the higher droplet concentrations. For a ship-relative wind speed of 10 m s^{-1} and a plume width of 20 km the number of particles injected for both simulations represents a particle production rate by the ship of 10^{17} s^{-1}. This production rate exceeds by a factor of 5 the source strength estimated by *Hindman et al.* [1994] for a ship that produced a ship track. The increased source strength in both simulations was imposed to compensate for the likely underactivation of CCN by the model.

In the type 1 ship track simulation, particles were injected 30 hours after the start of the simulation; in the type 2 ship track run, particles were injected at 24 hours. Although both sets of measurements were made around the same time of day, different injection times were used because there was a greater length of ship track upwind of the type 2 measurements (~200 km) than in the type 1 measurements (~40 km).

Comparisons between the control runs and the ship track runs for both types of ship tracks follow. The type 2 simulations are presented first because this type of ship track is more common, also more detailed measurements for comparison with model results are available.

4.3. Results of Model Simulations of Type 2 Ship Tracks

The evolution of the cloud liquid water distribution for the control run is shown in Figure 3a. Because of an upward flux of water vapor, water condenses in the boundary layer after ~2 hours of simulated time. This initial condensation releases a significant amount of latent heat, thereby generating buoyancy and mixing even more vapor upward. Within ~2 hours of this "shock" to the model due to cloud formation, drizzle increases, which reduces the liquid water content of the modeled cloud layer. By ~1200 (noon) the model has recovered from the shock of cloud formation and is responding to the diurnal cycle of solar radiation. Under the conditions of low wind speeds (~5 m s^{-1}) and moderate sea

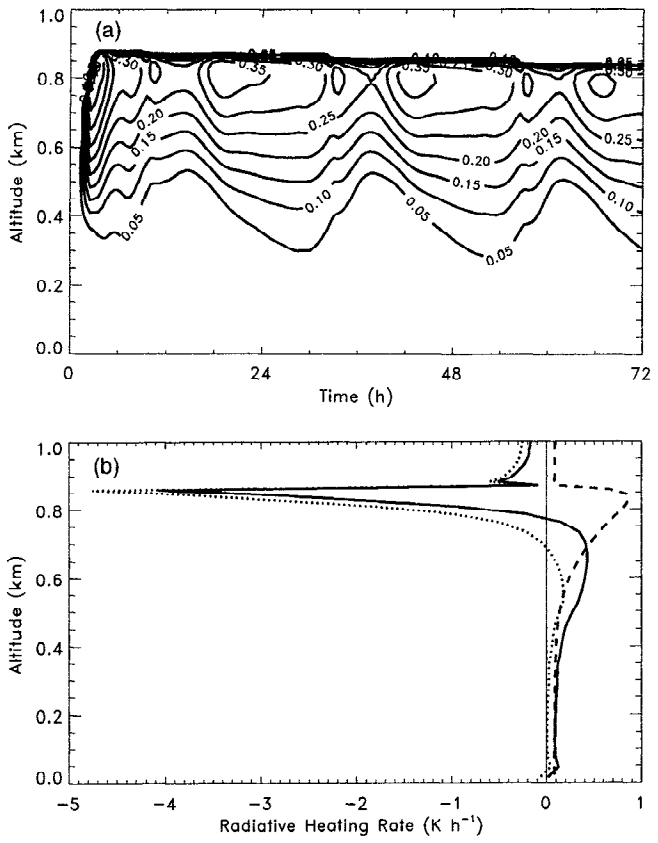

Figure 3. (a) Time evolution of liquid water mixing ratio (in grams per kilogram) in the control run (ambient cloud) for the type 2 ship track simulation. (b) Radiative heating rates for the control run (ambient cloud) at 12 hours. The dotted line is longwave heating, the dashed line is shortwave heating, and the solid line is net radiative heating.

surface temperature (17°C), turbulent mixing in the simulated boundary layer is driven primarily by longwave radiative cooling at cloud top. Solar heating offsets some of the cloud-top radiative cooling and contributes to radiative heating at cloud base (Figure 3b). The reduction of net cloud-top cooling during the day results in decreased mixing in the cloud layer. Solar radiative heating at cloud base reinforces longwave heating in that region and stabilizes the cloud with respect to the subcloud layer, thereby reducing turbulent mixing between the cloud and the subcloud layers. This reduction in mixing (referred to as "decoupling") limits the supply of moisture to the cloud and results in a lifting of cloud base during the afternoon. The diurnal cycle of mixing also results in a diurnal cycle of peak supersaturation due to the diurnal variation in the upward supply of vapor to the cloud layer. The peak supersaturation in the control run reaches ~0.06% at night and falls to ~0.04% in the afternoon.

Further cloud properties from the control run are shown in Figure 4. For comparison with the measurements of *Radke et al.* [1989] the modeled total droplet concentration (N_{drops}), liquid water content (q_l), and droplet effective radius (r_{eff}) are taken at 730 m altitude. The "shock" of cloud formation is evident, as are the recovery and subsequent diurnal cycles. The diurnal cycle of N_{drops} is driven by the diurnal cycle of supersaturation, while the diurnal cycle of q_l is driven more directly by the diurnal cycle of turbulent mixing. The diurnal cycle of r_{eff} responds to the combined cycles of N_{drops} and q_l: r_{eff} reaches a maximum of ~17 μm at night when q_l peaks and a minimum of ~14.5 μm in the afternoon when q_l is a minimum. The predicted diurnal trend of r_{eff} is supported by the satellite retrieval measurements of *Luo et al.* [1994], who found that the average value of r_{eff} for a sample of marine stratocumulus clouds off the coast of South America increased from 9.3 μm in the daytime measurements to 10.2 μm at night. The albedo of the cloud layer, which is shown in Figure 4d, is calculated using a fixed solar zenith angle of 60° (approximately the value when the ship tracks were measured) to eliminate the direct effect on albedo due to a changing solar angle. Changes in cloud albedo are thus determined by changes in cloud optical depth (not shown; it varies about a diurnal average of ~10), which are determined by variations in W and r_{eff} (see equation (1)). The diurnal cycle of W is not shown since it is in phase with the cycle of q_l; it ranges from ~70 g m^{-2} in the afternoon to ~130 g m^{-2} before dawn. Although the diurnal cycle of r_{eff} affects the cloud optical depth by reducing it at night, this reduction is overwhelmed by the opposite forcing due to the diurnal cycle of W. The W cycle dominates because W varies by ~50% (from its minimum value), while r_{eff} only varies by ~25%. The final aspect of the control run that we note here is that the diurnal cycle of drizzle (Figure 5) is in phase with the cycle of q_l (Figure 4c): drizzle is enhanced during the night and reduced during the day. Therefore drizzle responds to variations in q_l during the control run, rather than q_l responding to variations in drizzle.

As described in the preceding section, particles were injected into the model domain in the type 2 ship track run 24 hours after the start of the simulation. As seen in Figure 4a, a peak in N_{drops} is reached within 4 hours of the particle injection (the increase in N_{drops} results in a 50% reduction in the peak supersaturation). As seen in Figure 4b, the increase in N_{drops} leads directly to a decrease in r_{eff}. Smaller droplets produce less drizzle (Figure 5); because drizzle is a sink for liquid water (q_l), decreased drizzle allows q_l to initially increase (Figure 4c). This increase in q_l is consistent with the argument set forth by *Albrecht* [1989]. All of these changes contribute to an enhanced albedo of the cloud layer (Figure 4d), which was produced by an increase in cloud optical depth in the ship track run (at 30 hours, cloud optical depth in the ship track run is 20, while it is 12 in the control run). Table 2, which compares the cloud properties of the control run and the ship track run at 32 hours with the "uncontaminated" cloud and the "ship-contaminated" clouds measured by *Radke et al.* [1989] and *King et al.* [1993] around 0800 local standard time, shows that the model reproduces the measured trends. Although the values of r_{eff} predicted by the model exceed the measured values (since there were some problems with the droplet-sizing instrument during the measurements, it is not known whether the discrepancies are due to instrumental error or deficiencies in the model simulation), the relative changes between ambient and perturbed conditions are consistent. The differences between the model-predicted and the measured values of r_{eff} contribute to the corresponding differences in cloud optical depths (the optical depth measurements were not made directly but were derived from the measurements as described by *King et al.* [1993]); however, the relative changes between ambient and perturbed conditions are consistent. Note that the measured cloud reflectivities are not directly comparable to the model-predicted albedos (although the relative changes are

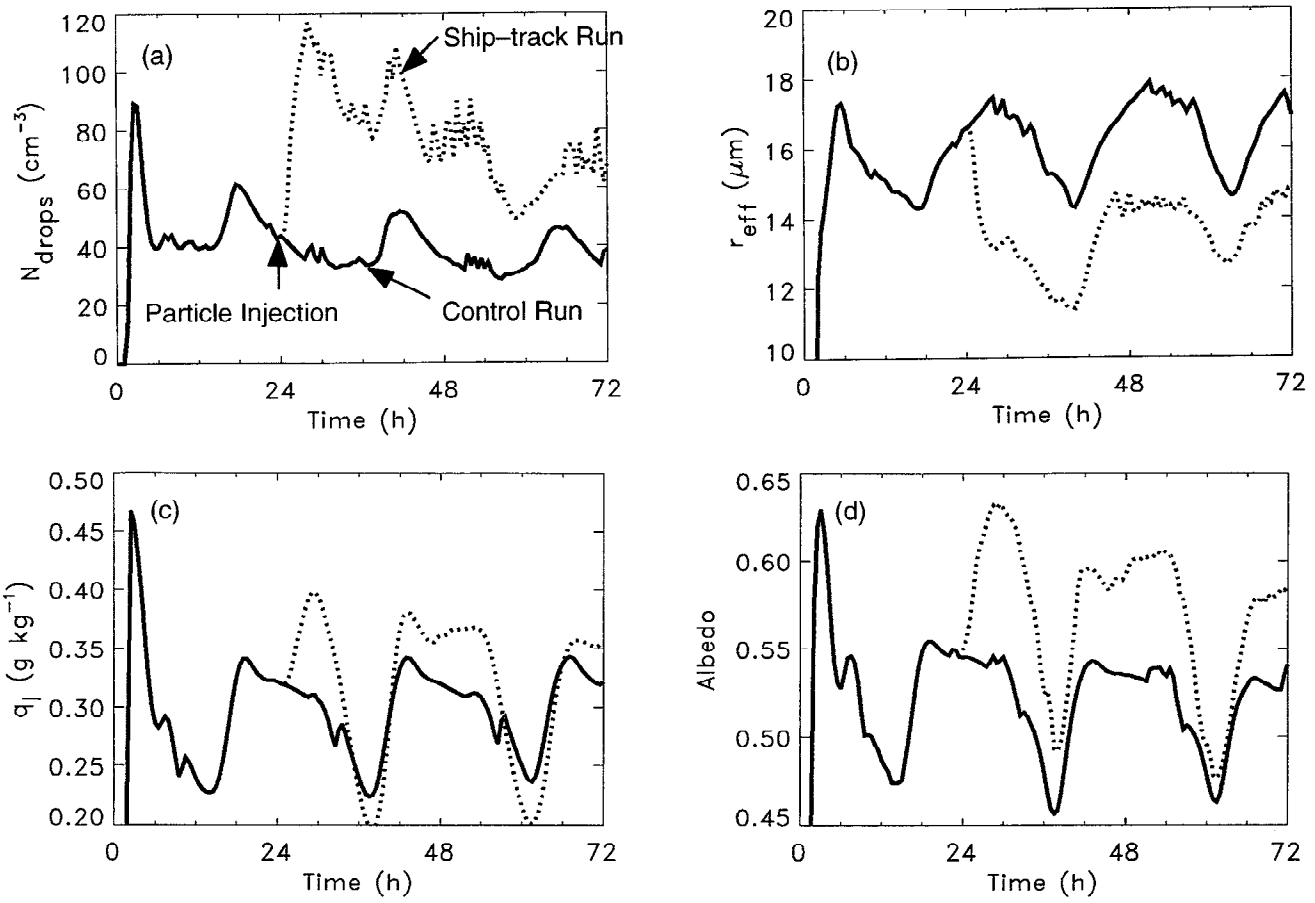

Figure 4. Model simulations of (a) total droplet concentration (N_{drops}), (b) droplet effective radius (r_{eff}), (c) liquid water mixing ratio (q_l), and top-of-atmosphere albedo at a wavelength of 0.6 μm (taken at a constant solar zenith angle of 60°). The values in Figures 4a, 4b, and 4c are at 730 m altitude. The solid lines are for the control run (ambient cloud) and the dotted lines are for the type 2 ship track simulation.

comparable) because the reflectivity is determined from the measured upwelling radiation at the observing angle of the satellite, whereas albedo is calculated from the ratio between the hemispherically averaged upward and downward fluxes.

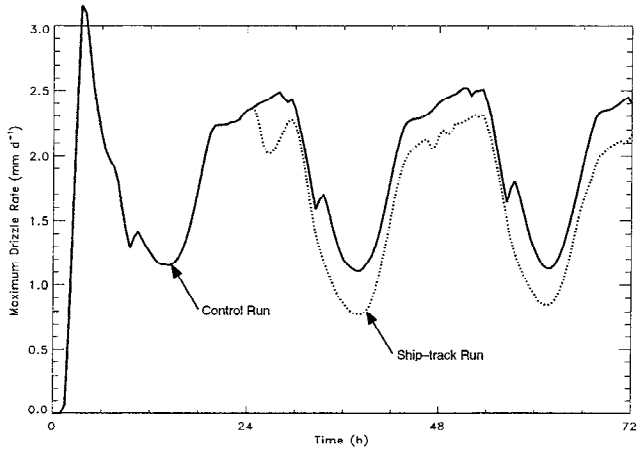

Figure 5. Model simulations of maximum drizzle rates, where the maximum drizzle rate is the peak value in the vertical profile of precipitation. The solid line is for the control run (ambient cloud) and the dotted line is for the type 2 ship track run.

The increased cloud water in the ship track run at 32 hours results in greater longwave cooling at cloud top, which leads to increased turbulent kinetic energy in the cloud layer at that time (Figure 6a). Measurements of turbulent kinetic energy in type 2 ship tracks (and in the surrounding regions) are needed to evaluate whether or not this model prediction is realistic.

The model predicts an enhancement of cloud liquid water during the morning and night, but in the afternoon it predicts less liquid water in the ship track run than in the control run. The relative reduction of q_l results from a greater decoupling between the cloud and the subcloud layers in the ship track run in the afternoon, as seen in the profiles of turbulent kinetic energy (TKE) at 36 hours (Figure 6b) where the reduced value of the minimum TKE below cloud base indicates a greater degree of decoupling in the ship track run. The greater decoupling in the afternoon in the ship track run is due to an increased rate of evaporation below cloud base. The increased evaporation is produced by differences in the droplet distributions that are transported below cloud (by turbulent mixing and sedimentation): in the ship track run the total droplet surface area is greater (because of the greater total droplet concentrations and the corresponding smaller average sizes of the droplets). The increased droplet surface area allows evaporation to occur more rapidly below cloud base. This increased evaporation does not result in a decoupled boundary layer at night, but it does allow a greater decoupling

Table 2. Comparison of Model Simulations of Microphysical and Optical Properties of a Type 2 Ship Track (8 hours After Particle Injection) With Measurements by *Radke et al.* [1989] and *King et al.* [1993] of a Type 2 Ship Track

Parameter	Measurements		Model Results	
	Ambient Cloud	Cloud Affected by Ship Emissions	Control Run for Ambient Cloud	Cloud Affected by Ship Emissions
Microphysical Properties at 730 m Altitude				
Droplet concentration, cm^{-3}	40	120	33	97
Droplet effective radius, μm	11.2	7.5	17	13
Liquid water content, $g\ m^{-3}$	0.30	0.45	0.32	0.40
Optical Properties				
Optical depth at 0.744 μm	20	44		
Optical depth at 0.6 μm			10	18
Reflectivity at 0.63 μm	61	68		
Albedo at 0.6 μm			52	62

to occur when solar heating reduces mixing in the boundary layer. The increased decoupling in the afternoon in the ship track run (and the associated decrease of cloud water) contradicts the arguments of *Albrecht* [1989], who reasoned that decreased drizzle should diminish the degree of decoupling in the boundary layer. However, Albrecht's argument is consistent with our model results during the morning and night.

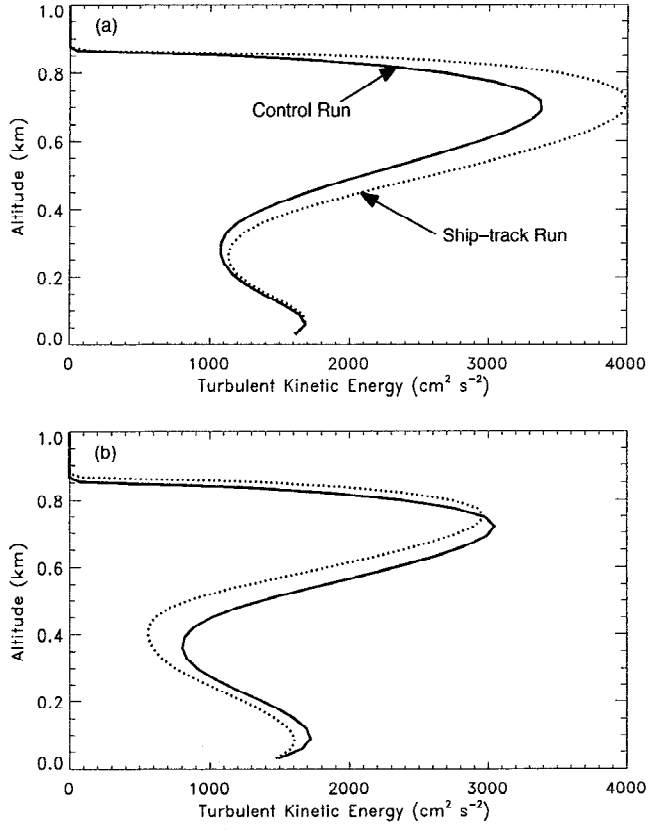

Figure 6. Model simulations of turbulent kinetic energy at (a) 32 and (b) 36 hours. The solid lines are for the control run (ambient cloud) and the dotted lines are for the type 2 ship track run.

Although the cloud water in the ship track run is reduced from that in the control run during the afternoon, the cloud albedo in the ship track run does not fall below that in the control run, because the relative change in r_{eff} dominates the relative change in W (Figure 4). However, the enhancement in cloud albedo in the ship track run does fall to a minimum in the afternoon.

A comparison of droplet size distributions at 730 m altitude in the control and ship track runs is shown in Figure 7. At both times shown (32 and 36 hours), the direct effect of particle injection is evident in the increases in droplet concentration for $r \lesssim 20$ μm. These increases result in the peaks of the number distributions shifting to smaller sizes in the ship track run; the decrease of r_{eff} in the ship track run (Figure 4b) corresponds to these shifts to smaller sizes. The increased concentrations of small droplets also results in a somewhat narrower droplet size distribution in the ship track run. The narrower distributions produce a reduction in the rate at which droplets coalesce to form droplets $\gtrsim 20$ μm in radius. The decrease in droplet coalescence results in reduced droplet concentrations for $r > 15$ μm at 36 hours (Figure 7b), but the reduction in droplet concentrations at 32 hours is limited to 20 μm $< r <$ 70 μm (Figure 7a). The decreased droplet concentrations for $r \gtrsim 20$ μm is consistent with the measurements of *Radke et al.* [1989]. However, the increased droplet concentrations for $r > 70$ μm at 32 hours is not supported by the measurements (taken at the corresponding time of 0800 local standard time). In the model simulations the increase in droplet concentrations for $r > 70$ μm at 32 hours is due to the relative increase in turbulent mixing at that time in the ship track run (Figure 6a), since turbulent mixing opposes the sedimentation of large droplets. By 36 hours, when turbulent mixing is reduced throughout the boundary layer in the ship track run (Figure 6b), there is no increase of droplet concentrations for $r > 15$ μm. These time-dependent changes in the concentrations of large droplets, which are not supported by measurements, could be an artifact of the model simulations.

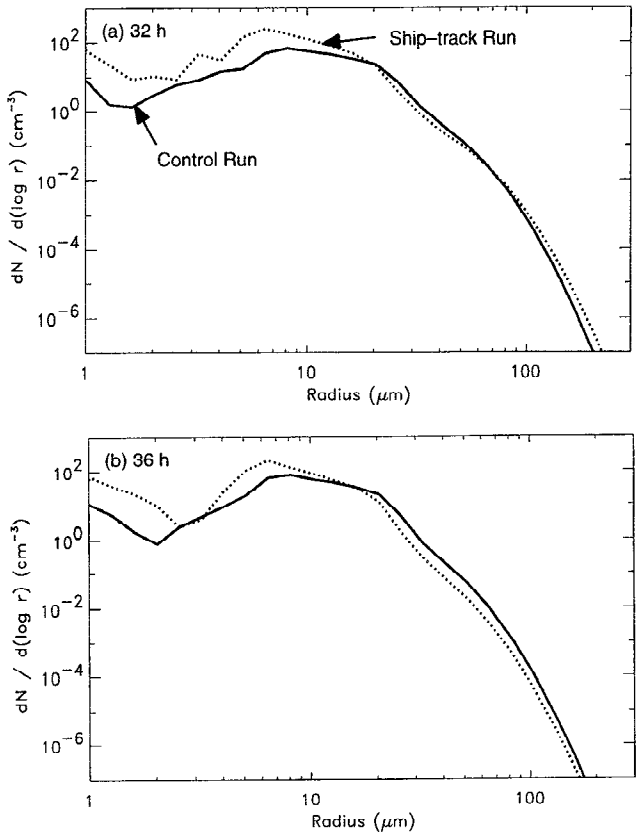

Figure 7. Model simulations of cloud droplet size distributions at 730 m altitude at (a) 32 and (b) 36 hours. The solid lines are for the control run (ambient cloud) and the dotted lines are for the type 2 ship track simulation.

Because of the diurnal response of the change in q_l, and the time that it takes (in the morning) for q_l to be enhanced by particle injection (a few hours), there are injection times for which an increase in q_l will be delayed until evening (i.e., after the restoration of mixing following the enhancement of afternoon decoupling). In further model simulations we investigated the effects of varying the time of day that the particles were injected. When the particles were injected at 30 hours into the simulation (0600 local standard time), there was only enough time for a slight enhancement of liquid water in the ship track run before the onset of daytime decoupling, which reduced liquid water below that in the control run. When the particles were injected at 36 hours (local noon), there was no enhancement of liquid water in the ship track run until after sunset.

Scorer [1987] reported that ship tracks can persist for up to 36 hours. Our model simulations provide information on the time that it takes for a ship track to dissipate (because of vertical removal processes such as droplet coalescence and surface deposition). For the atmospheric conditions and particle injection strength that we have simulated, it takes ~17 hours (after the peak droplet concentration is reached in the ship track run at 28 hours) for the perturbation in the cloud droplet concentration to fall to e^{-1} ($\simeq 0.37$) of its peak value. However, instead of falling farther, the perturbation in droplet concentration rises after sunset (at ~40 hours). This increase in the perturbation is attributable to a restoration of mixing between the cloud and the subcloud layers in the evening, which increases the supply of vapor to the cloud and results in an increased peak supersaturation (and hence droplet nucleation) in the ship track. Although there is a slight increase in droplet concentration after sunset in the control run, the increase is less pronounced because the daytime decoupling is less pronounced, and the reservoir of unactivated aerosol particles is reduced relative to the ship track run. Because of the increases in the perturbation of droplet concentration during the evenings, by the end of the model simulations (at 72 hours) the perturbation is still e^{-1} of its peak (44 hours after the peak was reached). By the end of the simulations the perturbation in albedo decreases to only one half of its peak value. Of course, in the real atmosphere, horizontal dispersion (due to vertical shear of the horizontal winds) and temporal variations in boundary conditions may reduce the lifetimes of ship tracks (as well as the lifetimes of the clouds in which the ship tracks are embedded) below the values we have calculated. However, in view of the long lifetimes we have estimated that there is no need to invoke enhanced gas-to-particle conversion well downwind of the ship to account for the persistence of ship tracks [*Radke et al.*, 1989].

The e-folding time for the perturbation in droplet concentration in the ship track run can be compared to the particle residence times calculated with this model under a different set of prescribed conditions (such as the minimum solar zenith angle). For a total particle concentration (the sum of unactivated aerosol particles and activated cloud droplets) of 120 cm^{-3}, *Ackerman et al.* [1994] calculated a particle residence time of ~12 hours. Because the residence time should represent an e-folding time of perturbations in particle concentration, the expected e-folding time for particle concentration is also 12 hours, which is much shorter than in the ship track run. Although, in the present simulations, the perturbation in the droplet concentration falls to half of its peak within 10 hours of reaching its peak, by the end of the simulations (44 hours after reaching the peak perturbation) the perturbation is still e^{-1} of its peak. As discussed above, the diurnal cycle of mixing in the boundary layer allows the elevated droplet concentrations in the ship track run to persist.

There are two related reasons why the e-folding time in these ship track simulations does not reproduce the particle residence time calculated for a different set of prescribed conditions by *Ackerman et al.* [1994]. First, the minimum solar zenith angle in their simulations was 35°, while the value here is 11°. Therefore the diurnal cycle of decoupling between the cloud and the subcloud layers in the simulations of *Ackerman et al.* [1994] was less pronounced than in the present simulations. Second, the size distribution of input aerosol particles in the simulations of *Ackerman et al.* [1994] was nearly monodisperse ($\sigma = 1.2$), whereas in the present simulations the size distribution of injected aerosol is broader ($\sigma = 1.6$). Hence in the simulations presented in this paper, when boundary layer mixing is restored at night (and the peak supersaturation rises), there are unactivated aerosol particles available for nucleation (which were not present in the narrower aerosol size distribution used by *Ackerman et al.* [1994]). This comparison of model results shows that particle residence times depend not only on particle concentrations but also on other factors, such as the minimum solar zenith angle and the width of the input aerosol size distribution.

4.4. Results of Model Simulations of Type 1 Ship Tracks

Ackerman et al. [1993] suggested that cloud-top radiative cooling cannot maintain mixing in the boundary layer when cloud droplet concentrations are very low ($\lesssim 5$ cm^{-3}). They found that when droplet concentrations fall to such low values, a stratocumulus-topped marine boundary layer can collapse to an optically thin, shallow fog layer. The cloud layer that develops in the control run of the type 1 ship track simulations is similar to that which results from such a collapse of the boundary layer, because droplet concentrations are very low (~5 cm^{-3}), cloud optical depth is only ~3, mixing in the boundary layer is driven by surface buoyancy, and the boundary layer is only ~450 m deep. Because this collapsed state results from low concentrations of CCN (and droplets) in the boundary layer, an injection of CCN can be expected to affect not only the cloud microphysical structure and optical properties in this case but also the turbulent structure of the boundary layer.

In the type 1 ship track simulations shown in Figure 8, the initial cloud formation in the particle deficient boundary layer "shocks" the model, the model then recovers, and subsequently undergoes moderate diurnal oscillations due to absorption of solar energy by the cloud. Because there is gnificantly less droplet surface area for condensation (compared to the control run for the type 2 ship track simulations), the peak supersaturation in the type 1 control run is much greater, oscillating between 0.27% during the day to 0.34% at night (not shown).

At 30 hours, particles are injected into the boundary layer for the type 1 ship track run. The increase in particles produces a dramatic increase in the concentration of cloud droplets (which results in an 80% reduction in the peak supersaturation), a reduction in r_{eff}, a rapid increase in liquid water, and a significant enhancement in cloud albedo (Figure 8). In the type 1 simulations the albedo increases from 33 to 50% (a relative increase of 50%, corresponding to an increase in cloud optical depth from 3 to 9), while in the type 2 simulations the albedo increases from 54 to 63% (a relative increase of 20%). This substantial difference in albedo perturbations further justifies our classification of ship tracks into two types. Furthermore, although the diurnal cycle of turbulent mixing was influenced by the particle injection in the type 2 ship track simulation, turbulent mixing was affected much more in the type 1 ship track simulation. This difference can be seen in Figure 9a, which shows a significant lifting of cloud base and a deepening of the boundary layer in

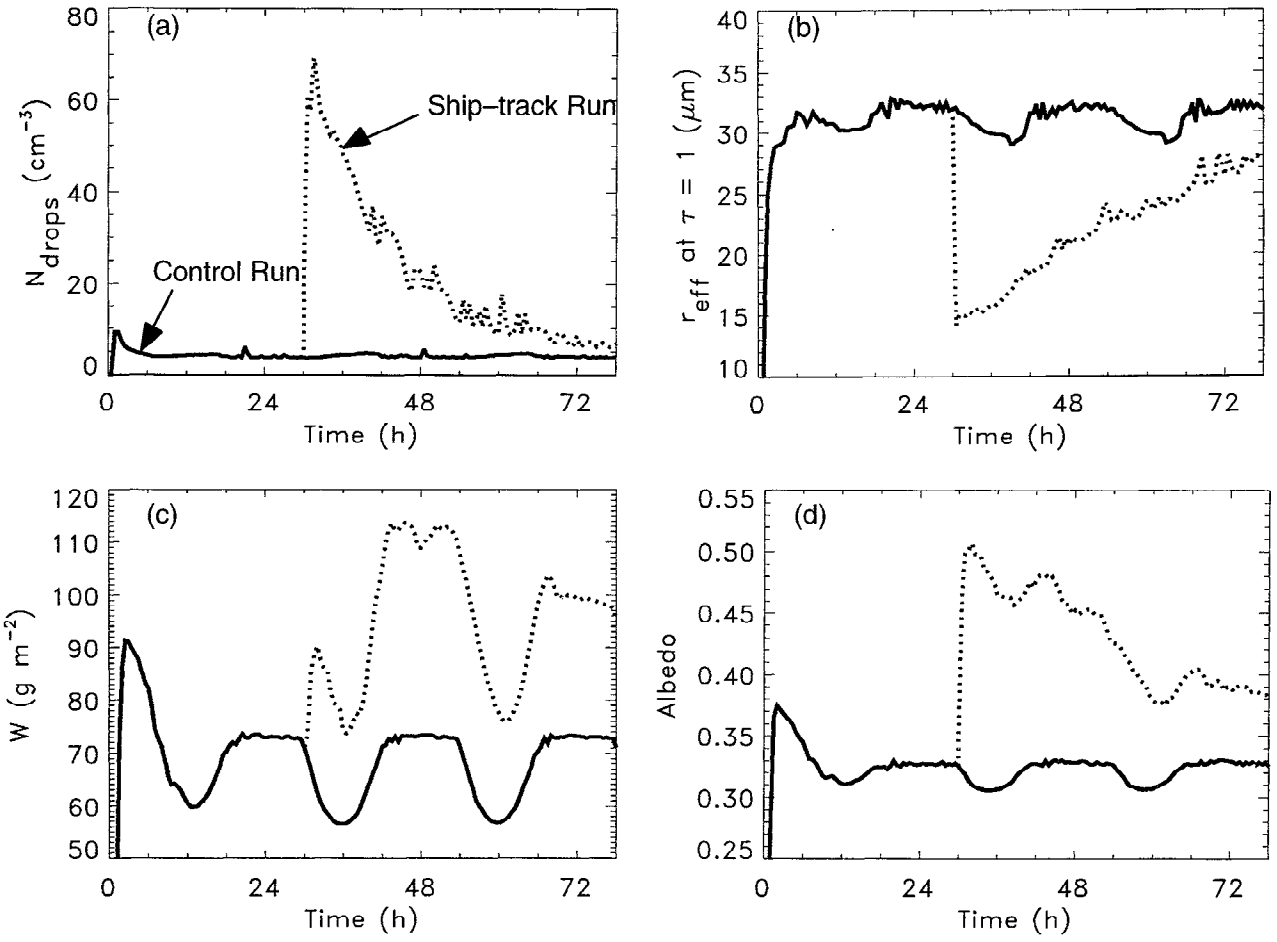

Figure 8. Model simulations of (a) total droplet concentration (N_{drops}) at cloud top, (b) droplet effective radius (r_{eff}) at an altitude corresponding to an optical depth of 1 below cloud top, (*c*) liquid water path (W), and top-of-atmosphere albedo at 0.6-μm wavelength (taken at a constant solar zenith angle of 60 °). The solid lines are for the control run (ambient cloud) and the dotted lines are for the type 1 ship track simulation.

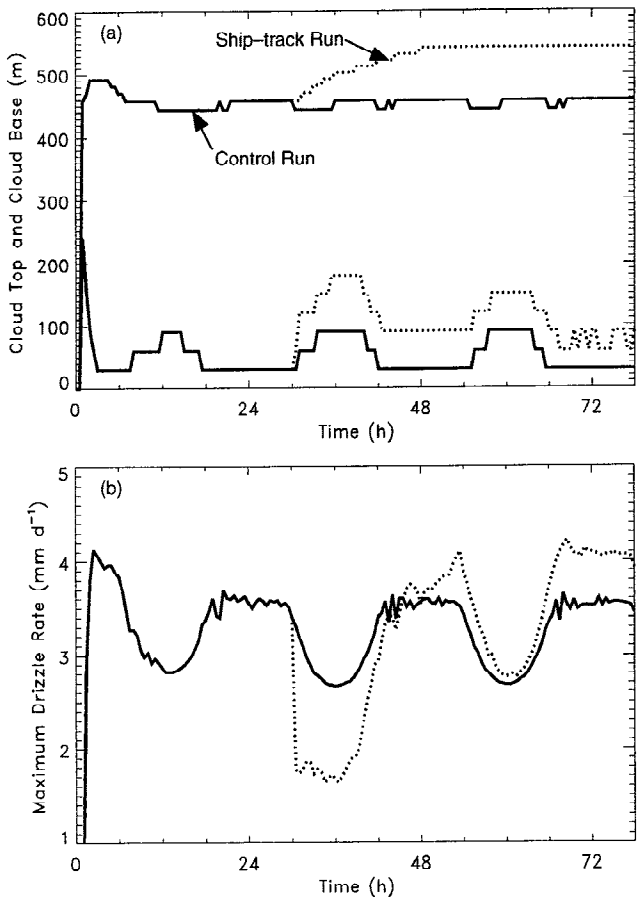

Figure 9. Model simulations of (a) cloud top and cloud base altitude and (b) the maximum drizzle rate (the peak value in the vertical profile of precipitation). Cloud-top and cloud base altitudes are defined by the locations at which visibility is < 1 km. The solid lines are for the control run (ambient cloud) and the dotted lines are for the type 1 ship track simulation.

the type 1 ship track simulation (in contrast, the boundary layer only deepened slightly during the type 2 ship track simulation, as seen in Figure 6b).

One of the factors contributing to the increase in albedo in the type 1 ship track simulation is the increase in cloud water (Figs. 8c and 10a). As in the type 2 case during morning and night, this increase is correlated with the initial decrease in drizzle (Figure 9b). However, in the type 1 ship track simulation the increase in cloud water is also due to increased mixing throughout the boundary layer, as seen in the profiles of turbulent kinetic energy at 33 hours (Figure 10b). Because of the increased cloud water, boundary layer mixing in the ship track run is driven by cloud-top radiative cooling; in the control run, mixing is driven by surface buoyancy (Figure 10c). The increased buoyancy flux in the cloud layer results from an infrared cooling rate that is not only increased in magnitude but, more importantly, peaks at cloud top in the type 1 ship track simulation (Figure 10d). This positive feedback between cloud water and boundary layer causes the boundary layer to deepen (Figure 9a). The increase in cloud water that is sustained by the increased mixing eventually allows the maximum drizzle flux (the peak in the vertical profile of drizzle) in the type 1 ship track simulation to exceed that in the corresponding control run (Figure 9b).

In the type 1 ship track simulation it takes ~12 hours for the perturbation in droplet concentration to fall to e^{-1} of its peak value (Figure 8a). However, it takes over twice as long for the albedo perturbation to decrease by e^{-1} (Figure 8d). The longer e-folding time for the albedo is due to the enhancement of cloud water in the ship track (Figure 8c), which persists longer than the perturbation in droplet concentration. In the subsequent 2 days of simulation the boundary layer does not collapse back to the depth it had prior to particle injection. This is because the droplet concentration does not reach the threshold value (~5 cm^{-3}) below which cloud-top radiative cooling cannot maintain vertical mixing [*Ackerman et al.*, 1993]. As in the type 2 ship track simulations these e-folding times probably represent maximum lifetimes for ship tracks.

In contrast to the type 2 ship track simulations the e-folding time that we have calculated for the perturbation in droplet concentration (~12 hours) in the type 1 ship track is nearly the same as that calculated by *Ackerman et al.* [1994] (for a total particle concentration of 70 cm^{-3}). The e-folding times are in agreement because the difference in solar zenith angles between our type 1 ship track simulations and the simulations of *Ackerman et al.* [1994] does not have an appreciable effect on the results in such a shallow boundary layer (decoupling between cloud and subcloud layers is favored in deeper boundary layers).

5. Conclusions

To investigate the phenomenon of ship tracks, we have used a numerical model to study the response of marine stratiform clouds to injections of particles into the marine boundary layer. The principal conclusions from this study can be summarized as follows.

1. Particle injections in the form of CCN can account for many of the features of ship tracks. Increased concentrations of CCN produce increased droplet concentrations that lead to increased droplet cross-sectional area and therefore increased cloud albedo. In addition, a decrease in average droplet size can reduce the drizzle rate. A reduction in the drizzle rate can increase the cloud liquid water, which leads to a further increase in cloud albedo.

2. We have proposed a classification of ship tracks into two types. Type 1 ship tracks stand out in visible satellite imagery, while type 2 ship tracks are only prominent in near-infrared imagery. The change in visible albedo for type 1 ship tracks is more pronounced than in type 2 ship tracks; in type 2 the albedo perturbations are masked by natural variability in cloud albedo. Our results suggest that the distinction between the two types of ship tracks is attributable to differences in the turbulent structure of the boundary layer preceding the injection of particles. The boundary layer conditions preceding the formation of a type 1 ship track can be described as a surface-driven fog (similar to the conditions that *Bowley* [1967] correlated with "anomalous cloud lines"). The conditions preceding the formation of a type 2 ship track can be described as a stratocumulus topped boundary layer in which mixing is driven primarily by cloud-top radiative cooling. The differences in boundary layer conditions are due to variations in ambient CCN concentrations: for type 1 ship tracks the ambient CCN concentrations are extremely low ($\lesssim$ 5 cm^{-3}), while for type 2 ship tracks the ambient CCN concentrations are higher.

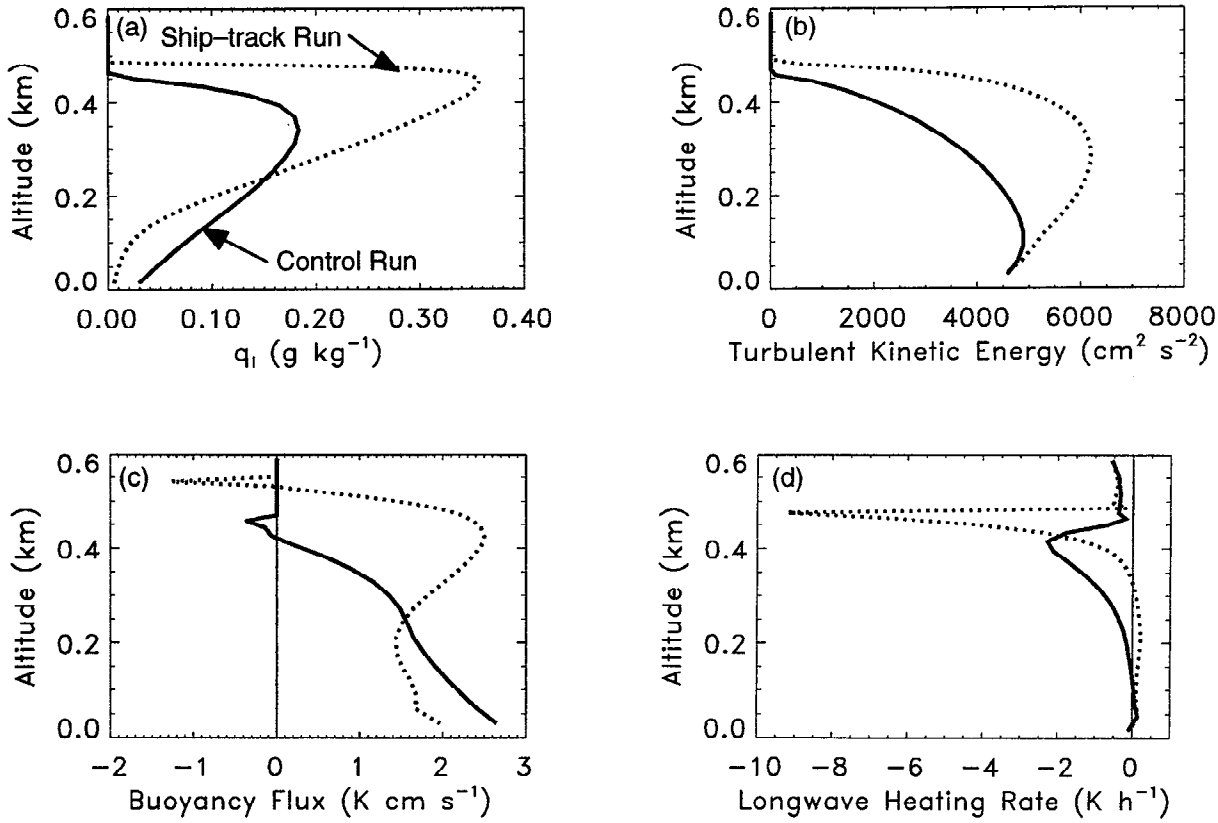

Figure 10. Model simulations at 33 hours of (a) liquid water mixing ratio (q_l), (b) turbulent kinetic energy, (*c*) buoyancy flux, and (*d*) longwave heating rate. The solid lines are for the control run (ambient cloud) and the dotted lines are for the type 1 ship track simulation.

3. Cloud liquid water does not always increase when the average size of cloud droplets decreases. During daytime the modeled cloud layer became more decoupled from the subcloud layer in the type 2 ship track simulation, thereby reducing the supply of moisture to the cloud layer. This reduction resulted in lower cloud water during the afternoon (relative to the control run). The greater susceptibility to decoupling is attributable to more rapid evaporation of droplets below cloud base.

4. The persistence of ship tracks is attributable to the dependence of the residence time of CCN on their concentrations. Because increased CCN concentrations produce smaller droplets that coalesce less efficiently, their removal rates (on a per particle basis) are decreased, and their residence times increased.

5. The lifetime of the type 2 ship track simulated by our model ($\gtrsim$ 2 days) exceeds that of observed ship tracks (up to 36 hours). This overestimation could be due to horizontal dispersion (which is not represented in our model) hastening the dissipation of ship tracks in the atmosphere. Changes in boundary conditions (e.g., large-scale subsidence, downwelling longwave radiative flux, sea surface temperature) may also disrupt ship tracks (and the surrounding clouds) and reduce their lifetimes.

Acknowledgments. We thank P. Durkee and K. Nielsen of the Naval Postgraduate School for providing the satellite imagery in Figure 1. This research was supported by NASA, ONR, DOE, and the National Science Foundation through grant ATM-9204149.

References

Ackerman, A. S., O. B. Toon, and P. V. Hobbs, Dissipation of marine stratiform clouds and collapse of the marine boundary layer due to depletion of cloud condensation nuclei by clouds, *Science*, *262*, 226-229, 1993.

Ackerman, A. S., O. B. Toon, and P. V. Hobbs, Reassessing the dependence of cloud condensation nucleus concentration on formation rate, *Nature*, *367*, 445-447, 1994.

Ackerman, A. S., O. B. Toon, and P. V. Hobbs, A model for particle microphysics, turbulent mixing, and radiative transfer in the stratocumulus-topped marine boundary layer and comparisons with observations, *J. Atmos. Sci.*, in press, 1995.

Albrecht, B. A., Aerosols, cloud microphysics, and fractional cloudiness, *Science*, *245*, 1227-1230, 1989.

Bowley, C. J., Comments on atmospheric requirements for the genesis of anomalous cloud lines, *J. Atmos. Sci.*, *24*, 596-597, 1967.

Coakley, J. A., Jr., R. L. Bernstein, and P. A. Durkee, Effect of ship track effluents on cloud reflectivity, *Science*, *237*, 1020-1022, 1987.

Conover, J. H., Anomalous cloud lines, *J. Atmos. Sci.*, *23*, 778-785, 1966.

Covert, D. S., North Pacific marine background aerosol: Average ammonium to sulfate molar ratio equals 1, *J. Geophys. Res.*, *93*, 8455-8458, 1988.

Duynkerke, P. G., and A. G. M. Driedonks: A model for the turbulent structure of the stratocumulus-topped atmospheric boundary layer, *J. Atmos. Sci.*, *44*, 43-64, 1987.

Hansen, J. E., and L. D. Travis, Light scattering in planetary atmospheres, *Space Sci. Rev.*, *16*, 527-610, 1974.

Hindman, E. E., Understanding ship-trail clouds, in *1990 Conference on Cloud Physics*, pp. 396-400, American Meteorological Society, Boston, Mass., 1990.

Hindman, E. E., W. M. Porch, J. G. Hudson, and P. A. Durkee, Ship-produced cloud line of 13 July 1991, in *Proceedings of the 11th International Conference on Cloud Physics and Precipitation*, pp. 184-187, Department of Meteorology, McGill University, Montreal, 1992.

Hindman, E. E., W. M. Porch, J. G. Hudson, and P. A. Durkee, Ship-produced cloud lines of 13 July 1991, *Atmos. Environ.*, *28*, 3393–3403, 1994.

Hudson, J. G., Cloud condensation nuclei near marine cumulus, *J. Geophys. Res.*, *98*, 2693-2702, 1993.

Hudson, J. G., and P. R. Frisbie, Cloud condensation nuclei near marine stratus, *J. Geophys. Res.*, *96*, 20,795-20,808, 1991.

King, M. D., L. F. Radke, and P. V. Hobbs, Optical properties of marine stratocumulus clouds modified by ships, *J. Geophys. Res.*, *98*, 2729-2739, 1993.

Lilly, D. K., Models of cloud-topped mixed layers under a strong inversion, *Q. J. R. Meteorol. Soc.*, *94*, 292-309, 1968.

Luo, G., X. Lin, and J. A. Coakley Jr., Eleven-micrometer emissivities and droplet radii for marine stratocumulus, *J. Geophys. Res.*, *99*, 3685-3698, 1994.

Nicholls, S., The dynamics of stratocumulus: Aircraft observations and comparisons with a mixed layer model, *Q. J. R. Meteorol. Soc.*, *110*, 783-820, 1984.

Nicholls, S., and J. Leighton, An observational study of the structure of stratiform cloud sheets, I, Structure, *Q. J. R. Meteorol. Soc.*, *112*, 431-460, 1986.

Porch, W. M., Kao, C. J., and Kelley, R. G., Ship trails and ship induced cloud dynamics, *Atmos. Environ.*, *24*(A), 1051-1059, 1990.

Radke, L. F., J. A. Coakley Jr., and M. D. King, Direct and remote sensing observations of the effects of ships on clouds, *Science*, *246*, 1146-1149, 1989.

Randall, D. A., J. A. Coakley, C. W. Fairall, R. A. Kropfli, and D. H. Lenschow, Outlook for research on subtropical marine stratiform clouds, *Bull. Am. Meteorol. Soc.*, *65*, 1290-1301, 1984.

Scorer, R. S., Ship trails, *Atmos. Environ.*, *21*, 1417-1425, 1987.

Toon, O. B., R. P. Turco, D. Westphal, R. Malone, and M. S. Liu, A multidimensional model for aerosols: Description of computational analogs, *J. Atmos. Sci.*, *45*, 2123-2143, 1988.

Toon, O. B., C. P. McKay, and T. P. Ackerman, Rapid calculation of radiative heating rates and photodissociation rates in inhomogeneous multiple scattering atmospheres, *J. Geophys. Res.*, *94*, 16,287-16,301, 1989.

Twomey, S., Pollution and the planetary albedo, *Atmos. Environ.*, *8*, 1251-1256, 1974.

Twomey, S., H. B. Howell, and T. A. Wojciechowski, Comments on "Anomalous cloud lines," *J. Atmos. Sci.*, *25*, 333-334, 1968.

Warren, S. G., C. J. Hahn, J. London, R. M. Chervin, and R. L. Jenne, Global distribution of total cloud cover and cloud type amounts over the ocean, *NCAR/TN 317 + STR*, 212 pp., Nat. Cent. for Atmos. Res., Boulder, Colo., 1988.

A. S. Ackerman and P. V. Hobbs, Department of Atmospheric Sciences, AK-40, University of Washington, Seattle, WA 98195. (e-mail: phobbs@atmos.washington.edu)

O. B. Toon, Space Science Division, NASA Ames Research Center, Moffett Field, CA 94035.

(Received May 2, 1994; revised December 6, 1994; accepted December 16, 1994.)